Bond particle model for semiconductor melts and its application to the liquid structure of germanium

1989 J. Phys.: Condens. Matter 1 1679

(http://iopscience.iop.org/0953-8984/1/9/013)

J. Phys.: Condens. Matter 1 (1989) 1679–1694. Printed in the UK

Bond particle model for semiconductor melts and its application to the liquid structure of germanium

A Ferrante† and M P Tosi‡

† International School of Advanced Studies, Trieste, Italy

‡ Department of Theoretical Physics of the University of Trieste and International Centre for Theoretical Physics, Trieste, Italy

Received 31 August 1988

Abstract. A simple type of liquid-state model is proposed to describe on a primitive level the melt of an elemental group IV semiconductor as a mixture of atoms and bond particles. The latter, on increase of a coupling strength parameter become increasingly localised between pairs of atoms up to local tetrahedral coordination of atoms by bond particles. Angular interatomic correlations are built into the model as bond particle localisation grows, even though the bare interactions between the components of the liquid are formally described solely in terms of central pair potentials. The model is solved for liquid structure by standard integral equation techniques of liquid-state theory and by Monte Carlo simulation, for values of the parameters which are appropriate to liquid germanium down to strongly supercooled states. The calculated liquid structure is compared with the results of diffraction experiments on liquid germanium near freezing and discussed in relation to diffraction data on amorphous germanium. The model suggests simple melting criteria for elemental and polar semiconductors, which are empirically verified.

1. Introduction

Simple models of interatomic forces have had an important role in advancing qualitative and quantitative understanding of condensed matter. In relation to properties of the liquid state, the fluids of neutral and charged hard spheres, the classical one-component plasma and the Lennard-Jones fluid have played such a role under two main aspects. Not only do they mimic classes of real fluids, but also provide simple test models for progress in statistical mechanics through joint theoretical and computer simulation studies.

Bond directionality is a qualitative feature of many real systems which is missing in the models mentioned above. It can be accounted for by invoking three-atom contributions to the model potential energy function in addition to pair potentials, as in the model proposed by Stillinger and Weber (1985) for computer simulation studies of crystalline and liquid silicon and used for amorphous silicon by various other authors (Luedtke and Landman 1988, and references therein). However, such models are hardly amenable to solution by current theoretical techniques, and indeed a more basic approach is now available for computer simulation of relatively simple covalent systems (Car and Parrinello 1988). Still at a modellistic level, alternatives to a many-body description of the potential energy function in fluids with highly directional forces can

0953-8984/89/091679 + 16 $02.50

nevertheless be expected to be useful. Thus, the model proposed by Smith and Nezbeda (1984), which relies on near-peripheral attraction sites to describe associated fluids, has been used in Monte Carlo studies of hydrogen bonding in water and methanol (Kolafa and Nezbeda 1987) and significant progress has been made in its solution by theoretical integral equation techniques (Wertheim 1988).

The Smith–Nezbeda model is naturally adapted to mimic phenomena of association and polymerisation occurring in hydrogen-bonded molecular fluids. It may possibly provide a useful starting point to deal with the network-like liquids and glasses formed by a number of ionic-semiconducting compound materials. The melting behaviour of group IV elemental and group III–group V polar semiconductors is however quite different (see for instance, Ubbelohde 1978). These crystallise at standard pressure in tetrahedrally coordinated open structures and a network-like amorphous state, having analogous local coordination and semiconducting properties, can be prepared for the elements by suitable laboratory techniques. Melting occurs with a shrinkage in specific volume, a marked increase in near-neighbour coordination and a change of electrical transport character to metallic-type conductivity. Such radical changes in atomic and electronic structure on melting can be viewed in a primitive chemical picture of bonding as associated with a release of valence electrons from interatomic bonds into conducting states.

The above elementary picture of semiconductor melting recalls to mind the bond charge model proposed by Phillips (1970) for crystalline elemental semiconductors (Ferrante *et al* 1988). The model represents the electronic charge distribution in each covalent bond as a point-like charge of suitable amount, localised at mid-distance between each pair of neighbouring atoms. The bond charges participate in the lattice dynamics and indeed an important application of the model has been its use in the calculation of phonon dispersion curves in crystalline semiconductors by Martin (1969) and several other authors (see for instance, Miglio *et al* 1988 for an application to surface phonons in silicon). Extension to a primitive model for the melt should allow freedom for Phillips' bond particles to leave the bond, though retaining the possibility of partial localisation up to a maximum of four bond particles around one atom.

Such a primitive model for semiconductor melts is explored in the present work with specific application to the liquid structure of germanium as a test case. The starting point is the well known model of a two-component liquid as a mixture of hard spheres (of very different sizes in the present case). The bond particle component is subject to localisation between pairs of atoms by attractions to the atomic component. Localisation is constrained by an upper limit of four on the local coordination of atoms by bond particles through non-additivity of hard-sphere diameters, by fixing a distance of closest approach between bond particles from the size of a tetrahedron inscribed in the atomic sphere.

The main aim in examining the model as formulated above is to follow the structural evolution of both the atomic (A) component and the bond particle (B) component as temperature is lowered from hot liquid states to strongly supercooled states. Directionality of effective atom–atom interactions and angular interatomic correlations, ultimately leading to fourfold coordination, are progressively built into the model as localisation of bond particles sets in and grows. Thus the model can offer some insight into disordered states of semiconductors, which is complementary to that gained from theories of their metallic melt based on effective atom–atom interactions from the electron theory of metals (Hafner and Kahl 1984) and from many-atom descriptions of the potential energy function (Luedtke and Landman 1988, and references therein).

Since only central pair potentials are formally involved in describing the A–A, A–B and B–B interactions, the model can be solved for liquid structure by standard integral

equation techniques of liquid-state theory. We examine its solution in the hypernetted chain approximation (HNC) and in one of its currently available refinements (HMSA) due to Zerah and Hansen (1986). We also present the results of Monte Carlo simulation runs, which test the quantitative accuracy of the above approximations in the previously untried context in which we are using them.

Equilibration of the simulation sample and reliable statistics after equilibration require uncommonly long Monte Carlo runs at relevant values of the model parameters. It is therefore advantageous to deal with a short-range type of A–B attraction. We study in the aforementioned detail a modification of Phillips' model in which the A–B attraction is given by a very localised potential well on the atom's surface, relying for this purpose on the analysis of phonon dispersion calculations given by Weber (1977). However, in anticipation of extensions to polar compounds, we examine in the HNC also a model of the melt which invokes only Coulomb interactions between the components of the fluid. In both cases the calculations cover a range of values for the ratio of A–B coupling strength to thermal energy which extends to strongly supercooled states of liquid germanium. The growth of bond particle localisation with growing A–B coupling proceeds with somewhat different modalities under pure Coulomb interactions as opposed to localised attractions. Nevertheless these two extreme alternatives yield consistent pictures for the liquid structure of germanium near freezing, at values of the A–B coupling strength which are in essential agreement with the known values of the bond charge in the crystal and of its valence–conduction band gap, respectively.

2. Presentation of the model

We consider a two-component fluid of hard spheres, with components A and B having number density n_A and $n_B = 2n_A$ at temperature T. The hard-sphere interactions are characterised by three distances of closest approach (σ_{AA}, σ_{AB} and σ_{BB}, say). In the problem at hand the relevant values of the hard-sphere contact distances are asked to satisfy the approximate relations $\sigma_{AA} \simeq 2\sigma_{AB} \leqslant d$, where d is the first-neighbour distance in the liquid, and $\sigma_{BB} \geqslant (2/3)^{1/2}\sigma_{AA}$. These relations imply that, even though the B component is essentially point-like compared with the A component, no more than four B particles can be found in immediate contact with any A particle. This feature of the model is to be contrasted with the primitive model of a liquid alloy as a mixture of hard spheres (Ashcroft and Langreth 1967, Enderby and North 1968), in which additivity of hard-sphere diameters is imposed by setting $\sigma_{AB} = (\sigma_{AA} + \sigma_{BB})/2$.

We next introduce interactions which lead to strong relative ordering of the two components in the liquid, considering two alternative cases. The first choice (localised attraction model (LAM)) introduces an attractive interaction between A and B particles in the form of a narrow potential well centred at a distance $d/2$ from the centre of each A particle and uniformly spread over its surface (see figure 1). The well is taken to have a Gaussian shape of half-width σ and depth V, with $\sigma \simeq \frac{1}{2}d - \sigma_{AB}$. The well depth V enters the model only in units of the thermal energy $k_B T$, yielding a coupling strength parameter $V^* = V/k_B T$ which will be allowed to increase continuously from zero in order to follow the process of localisation of the bond particles. For liquid germanium near freezing, estimating V from the valence–conduction band gap of the crystal at room temperature ($V \simeq 0.7$ eV), we anticipate $V^* \simeq 6$.

The second alternative that we explore for the origin of relative order of the components of the liquid is closer to Phillips' original bond charge model (BCM). The hard

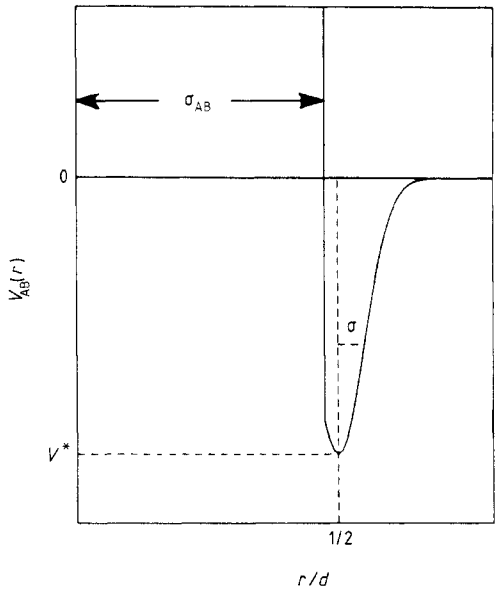

Figure 1. Atom-bond particle interaction potential versus distance in the LAM.

spheres are assigned charges in amounts $Z_A e$ and $Z_B e$ respectively, with $Z_B = -\frac{1}{2}Z_A$. The A–B coupling strength is now measured by the 'plasma parameter' $\Gamma = Z_B^2 e^2/(ak_B T)$, the length a being related to the liquid density by $a = (4\pi n_A)^{-1/3}$. Again this parameter will be allowed to increase continuously from zero in the calculations presented in § 5 below. Phillips' original estimate was $|Z_B| \simeq 0.5$ for germanium, corresponding to two electronic charges screened by the dielectric constant of the material, while fits of the phonon dispersion curves in crystalline germanium by Martin (1969) and Weber (1977) yield values of $|Z_B|$ equal to 0.65 and 0.40, respectively. The corresponding value for Γ appropriate to germanium near freezing is in the range 50–20.

A combination of Coulomb interactions and short-range attractions may actually turn out to be necessary in an extension of the model to polar semiconductors, which is otherwise easily envisaged in terms of adjustments in the distances of closest approach of the various components and of the equilibrium position for a bond particle. In relation to elemental semiconductors, we may comment at this point on the relationship between the two alternative treatments of ordering interactions that we are considering. The analysis given by Weber (1977) for phonon dispersion curves in the crystal is illuminating in this respect. He found only minor changes in the calculated dispersion curves upon replacing Coulomb and central interactions of ions and bond charges by short-range central and non-central interactions along one bond. His conclusion was that the long-range part of the Coulomb forces is unimportant. As we shall see, this conclusion still holds in the liquid near freezing. We may also explicitly note here that the role played in Weber's models by bond-bending and non-central forces is taken up in our model for the liquid, at appreciable values of the A–B coupling strength, by the simple requirement made on the distance of closest approach between bond particles.

The calculations reported below refer to two choices of the liquid density and first-neighbour distance, which are taken from experiments on germanium. For liquid germanium at $T = 1253$ K, which is somewhat above the freezing point at atmospheric

Table 1. Sets of model parameters used in the calculations.

	n_A (Å^{-3})	d (Å)	σ_{AA}/d	σ_{AB}/d	σ_{BB}/d	σ/d
Set 1	0.0461	2.63	0.94	0.475	0.80	0.050
Set 2	0.0429	2.46	0.95	0.475	0.76	0.050
Set 3	0.0429	2.46	0.98	0.475	0.81	0.050
Set 4	0.0429	2.46	0.98	0.500	0.81	—

pressure, one has $n_A = 0.0461$ Å^{-3} (Glazov *et al* 1969) and $d = 2.63$ Å from the neutron diffraction experiments of Gabathuler and Steeb (1979). In amorphous germanium, on the other hand, the density depends on film deposition rate and on film thickness, being at most equal to 97% of the crystalline density (see for instance, Viscor 1988). We have considered such a value of the density ($n_A = 0.0429$ Å^{-3}) as our second choice, in combination with the value $d = 2.46$ Å from the diffraction experiments of Etherington *et al* (1982) on amorphous germanium at room temperature. This value of the first-neighbour distance is practically the same as in the crystalline phase. Finally, the various choices that we shall illustrate for the hard-sphere contact distances and the well half-width, within the prescriptions noted earlier in this section, are collected for convenience in table 1. We shall comment later on these specific choices as the opportunity arises.

3. Solution of the model for the liquid structure

The liquid structure of the model is described by the partial pair distribution functions $g_{\alpha\beta}(r)$, which are defined as usual by setting equal to $4\pi r^2 n_\beta g_{\alpha\beta}(r)\,dr$ the number of particles of type β (with β = A or B) within a spherical shell at distance r from a particle of type α (with α = A or B). The partial structure factors $S_{\alpha\beta}(k)$ are then given by

$$S_{\alpha\beta}(k) = \delta_{\alpha\beta} + 4\pi(n_\alpha n_\beta)^{1/2} \int_0^\infty h_{\alpha\beta}(r) \exp(i\boldsymbol{k}\cdot\boldsymbol{r})\, r^2\, dr \tag{1}$$

where $h_{\alpha\beta}(r) = g_{\alpha\beta}(r) - 1$. The direct correlation functions $c_{\alpha\beta}(r)$ are further introduced through the Pearson–Rushbrooke integral equations

$$h_{\alpha\beta}(r) = c_{\alpha\beta}(r) + \sum_\gamma n_\gamma \int c_{\alpha\gamma}(|\boldsymbol{r} - \boldsymbol{r}'|)\, h_{\gamma\beta}(r')\, d\boldsymbol{r}'. \tag{2}$$

The cumulative coordination numbers $N_{\alpha\beta}(R)$ are calculated from the integrals

$$N_{\alpha\beta}(R) = 4\pi n_\beta \int_0^R g_{\alpha\beta}(r)\, r^2\, dr. \tag{3}$$

The near-neighbour coordination numbers $N_{\alpha\beta}$ that we shall report are obtained by making the integration limit R equal to the position of the first minimum in the corresponding $g_{\alpha\beta}(r)$.

Solution of the model for increasing values of the coupling strength V^* or Γ is first found in the HNC. This imposes on the integral equations (2) the approximate closure

$$g_{\alpha\beta}(r) = \exp(-\Phi_{\alpha\beta}(r) + h_{\alpha\beta}(r) - c_{\alpha\beta}(r)) \tag{4}$$

where $\Phi_{\alpha\beta}(r)$ are the pair potentials in units of $k_B T$. Of course, the hard-sphere part of

the pair potentials simply leads to $g_{\alpha\beta}(r) = 0$ for $r < \sigma_{\alpha\beta}$. The method followed for the numerical solution of the combined sets of equations (2) and (4) is that developed for two-component charged liquids by Abernethy and Gillan (1980). Special attention is taken in handling the discontinuities introduced in the direct correlation functions at contact by the hard-sphere part of the interactions. Our calculations adopt a set of eight basis functions for an approximate representation of the functions $h_{\alpha\beta}(r) - c_{\alpha\beta}(r)$, combined with refinement on a mesh of 516 points with spacing equal to $0.02a$. A suitably large range of wavenumber k must be adopted for Fourier transforms being taken during the iterative numerical solution at large values of the A–B coupling strength, where the partial structure factors show relatively long-range oscillations.

The solution of the LAM is also sought in the HMSA, which improves on the HNC closure by combining it with a modified mean spherical approximation at short interparticle distances (Zerah and Hansen 1986). Precisely, equation (4) is replaced by

$$g_{\alpha\beta}(r) = \exp(-\Phi^{(1)}_{\alpha\beta}(r)) \left(1 + \frac{\exp[f_{\alpha\beta}(r)(h_{\alpha\beta}(r) - c_{\alpha\beta}(r) - \Phi^{(2)}_{\alpha\beta}(r))] - 1}{f_{\alpha\beta}(r)}\right) \tag{5}$$

where $\Phi^{(1)}_{\alpha\beta}(r)$ denotes the repulsive part of the pair potentials, $\Phi^{(2)}_{AB}(r)$ is the attractive part of the A–B pair potential shown in figure 1, and $\Phi^{(2)}_{AA}(r) = \Phi^{(2)}_{BB}(r) = 0$. Further, the mixing functions $f_{\alpha\beta}(r)$ have the form

$$f_{\alpha\beta}(r) = 1 - \exp(-br/\sigma_{\alpha\beta}) \tag{6}$$

and the parameter b is to be determined by imposing consistency between the virial compressibility and the compressibility from the thermodynamic fluctuation formula. The numerical method of solution of (2) and (5) is the same as used in the HNC.

Finally, the solution of the LAM is also found by a canonical-ensemble Monte Carlo simulation method over a wide range of values for the A–B coupling strength. The simulation sample consists of 64 particles of type A and 128 particles of type B in a box of side $L = 9.2996a$ with periodic boundary conditions. The system is started on a diamond structure at $V^* = 1$ and allowed to equilibrate itself into a disordered state over 10^6 steps, the behaviour of the density fluctuation variables at the (1,1,1) Bragg reflection being monitored during this process. The pair distribution functions $g_{\alpha\beta}(r)$ are then sampled at a series of increasingly larger values of V^* with a statistics built from 10^6 steps following successive equilibrations lasting 10^6 steps. Each equilibration process is started from the equilibrium configuration appropriate to the preceding value of V^* and is followed by monitoring the pressure and the internal energy. The limited size of the sample limits reliable information to the first two interatomic coordination shells.

4. Results for the LAM

Figure 2 shows the partial pair distribution functions and the partial structure factors as calculated in the HNC for coupling strength V^* equal to zero. These results are the starting point of all our liquid-structure calculations and can be compared with liquid structure in additive models for mixtures of hard spheres with very different diameters, for both neutral fluids (Ashcroft and Langreth 1967) and charged fluids (Gillan *et al* 1976). In both these cases some degree of relative order of the two components is signalled by a valley in $S_{AB}(k)$ in approximate correspondence with the main peak in $S_{AA}(k)$, while $S_{BB}(k)$ (the structure factor for the small-sized component) is essentially featureless. As

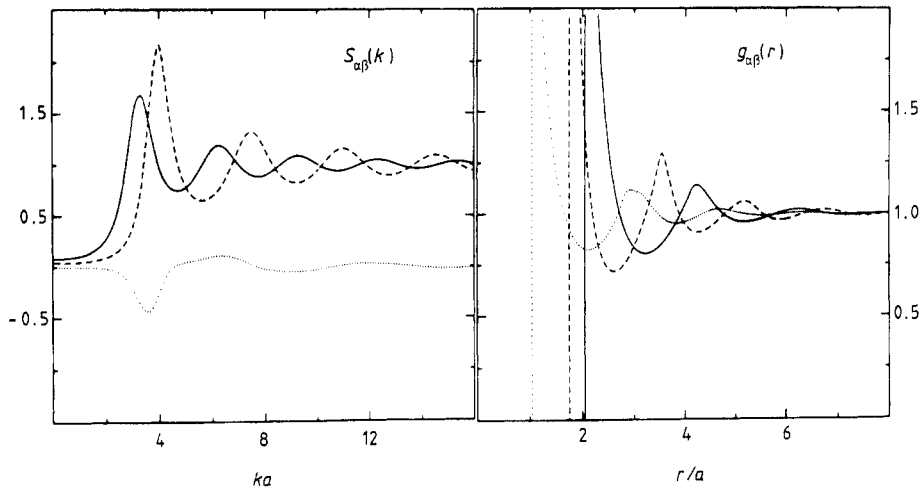

Figure 2. Partial structure factors $S_{\alpha\beta}(k)$ (left) and pair distribution functions $g_{\alpha\beta}(r)$ (right) for the LAM (set 1) at $V^* = 0$ in the HNC. Full curves, A–A correlations; dotted curves, A–B correlations; broken curves, B–B correlations.

is evident from figure 2, our choice of σ_{BB} from the tetrahedron rule builds sharp structure in $S_{BB}(k)$ and in $g_{BB}(r)$, while it preserves and indeed somewhat strengthens the relative order of the two components. Localisation of B particles is nevertheless absent. This is clearly shown by the high value attained by $g_{AB}(r)$ at its main minimum, which reflects essentially free exchange of B particles among their first and second coordination shells around A particles.

4.1. Localisation of bond particles and the structure of liquid germanium

Table 2 shows how localisation of B particles proceeds in the HNC with increasing V^* at constant density and the structural changes that it induces in the A component of the liquid. The degree of localisation can be gauged through the coordination number N_{AB}, the position R_{AB} of the main minimum in $g_{AB}(r)$, and the value of $g_{AB}(R_{AB})$. Table 2 reports these values as well as those appropriate to the same quantities for A–A and B–B pairs.

Two rapid changes in structural behaviour are seen to occur in narrow ranges of V^* as this parameter is increased. Firstly, for V^* in the range 1–2 there is a rapid drop of N_{AB}, from $N_{AB} \simeq 5.5$ to $N_{AB} \simeq 2.7$, as well as in R_{AB}, from $R_{AB} \simeq 0.9d$ to $R_{AB} \simeq 0.6d$. Recalling the definition of N_{AB} given in § 3, incipient localisation of B particles is occurring in the region of near-contact with A particles, although exchange with the surrounding liquid is still quite free ($g_{AB}(R_{AB}) \simeq 0.8$). Henceforward, localisation grows with increasing V^* through a slow increase in N_{AB} and a fairly rapid drop in $g_{AB}(R_{AB})$, while R_{AB} remains essentially constant. The next rapid change in structural behaviour occurs for V^* in the range 6–7. Here, R_{AA} drops rapidly from $R_{AA} \simeq 1.5d$ to $R_{AA} \simeq 1.2d$ and N_{AA} drops by essentially a factor of two to $N_{AA} \simeq 6.8$. Evidently, localisation of B particles has become sufficiently strong that the first A–A coordination shell is being split into two shells. At this point the A–A pair distribution functions start to resemble qualitatively the observed $g_{GeGe}(r)$ in real liquid germanium, having locally the shape of two neighbouring coordination shells separated by a shallow minimum and with a first

Table 2. Coordination numbers and properties of the main minimum in the HNC pair distribution functions for the LAM.

V^*	N_{AB}	R_{AB}/d	$g_{AB}(R_{AB})$	N_{AA}	R_{AA}/d	$g_{AA}(R_{AA})$	N_{BB}	R_{BB}/d	$g_{BB}(R_{BB})$
Liquid density, set 1									
0	6.48	0.97	0.82	10.5	1.47	0.81	11.3	1.19	0.72
0.5	6.03	0.94	0.83	10.5	1.47	0.81	11.3	1.19	0.71
1	5.46	0.91	0.84	10.3	1.46	0.82	11.3	1.19	0.71
2	2.66	0.67	0.77	10.3	1.46	0.83	11.2	1.18	0.70
3	2.67	0.64	0.55	10.4	1.46	0.85	10.9	1.17	0.69
4	2.77	0.64	0.37	10.6	1.47	0.87	10.5	1.15	0.68
5	2.88	0.63	0.25	11.0	1.49	0.90	10.2	1.14	0.67
6	3.01	0.63	0.16	12.4	1.55	0.92	9.96	1.12	0.65
7	3.12	0.63	0.099	6.85	1.28	0.94	9.76	1.11	0.62
7.5	3.17	0.63	0.078	6.53	1.24	0.94	9.75	1.11	0.62
8	3.21	0.63	0.061	5.94	1.22	0.93	9.58	1.10	0.61
10	3.36	0.63	0.023	5.37	1.19	0.86	9.39	1.07	0.58
14	3.57	0.63	0.0029	5.04	1.16	0.86	9.07	1.07	0.52
18	3.71	0.63	0.0006	5.03	1.15	0.63	8.93	1.06	0.47
Amorphous density, set 3									
14	3.19	0.64	0.0023	4.36	1.24	0.84	7.16	1.10	0.60
18	3.35	0.64	0.0003	4.28	1.22	0.72	7.03	1.08	0.53

neighbour coordination of order 6.5–6.8 (Waseda and Suzuki 1975, Gabathuler and Steeb 1979, Waseda 1980).

It is also seen from table 2 that upon further increase of V^* the coordination number N_{AB} slowly moves towards the value 4, while localisation of B particles becomes essentially complete ($g_{AB}(R_{AB}) \simeq 0$). At the same time N_{AA} decreases steadily, but appears to approach the value 5 rather than 4 when the density is maintained equal to the liquid density. The B–B distribution function shows only a smooth variation throughout all these structural arrangements, with N_{BB} approaching the value $N_{BB} \simeq 9$ for $V^* \simeq 20$ at the liquid density. We note that the bond-centre–bond-centre coordination number in the ideal diamond structure is equal to 6.

In order to make contact with properties of amorphous germanium, it is crucial to take account of its reduced density. This is shown in the bottom part of table 2, which reports the final stages of the same structural evolution when followed at the appropriate density. The only qualitative changes are that now both N_{AB} and N_{AA} are approaching the value 4, from below and from above respectively, and that N_{BB} touches the value 7 at $V^* \simeq 20$. We also note that this value of the coupling strength is fairly low relative to what we would estimate for amorphous germanium at room temperature ($V^* \simeq 30$, taking into account $V^* \simeq 7$ for the freezing liquid and a drop of temperature by a factor 4). We shall return to this point in § 4.2 in discussing the limitations of the HNC.

The evolution of liquid structure with increasing V^* at constant density is also shown through the HNC partial structure factors in figure 3. Upon incipient localisation of B particles at $V^* \simeq 1$–2, the valley in $S_{AB}(k)$ is shifted towards the position of the main peak in $S_{BB}(k)$ and a prepeak grows in correspondence with the main peak in $S_{AA}(k)$. Splitting of the A–A first coordination shell into two shells at $V^* \simeq 6$–7 appears in $S_{AA}(k)$ as a new structure in the main peak, in the shape of a shoulder on its large-k side. A well known qualitative feature of the observed structure factor of liquid germanium is the

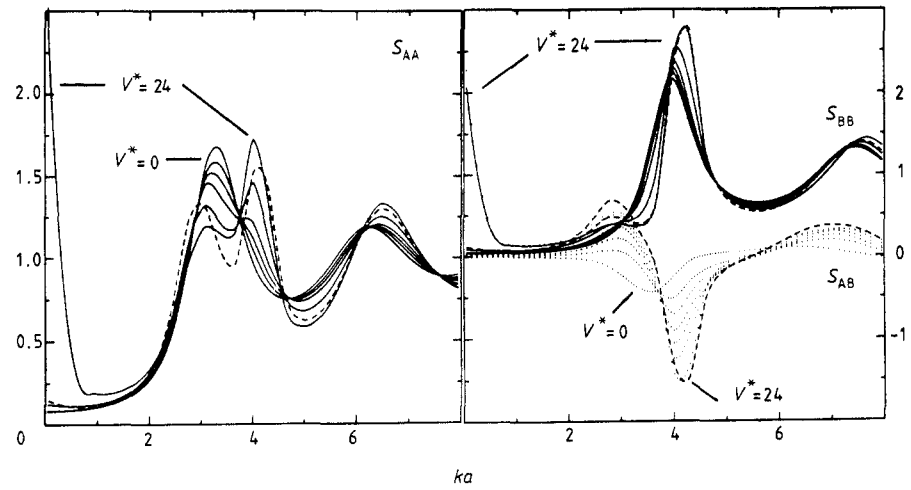

Figure 3. Partial structure factors $S_{AA}(k)$ (left), $S_{AB}(k)$ (right, dotted curves) and $S_{BB}(k)$ (right, full curves) for the LAM (set 1) in the HNC at a series of values of V^* ($V^* = 0, 3, 5, 7.5, 14$ and 24, the first and last values being marked in the figures). The broken lines give the HMSA results for $V^* = 24$ and $b = 1$.

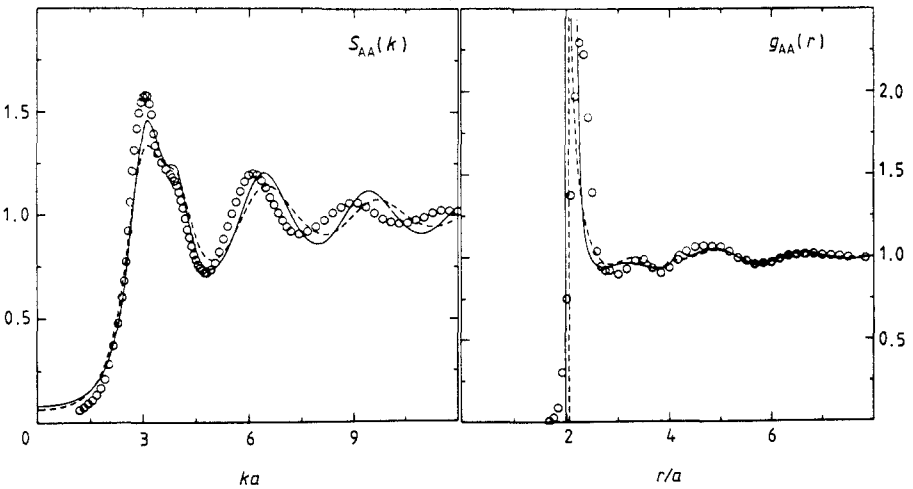

Figure 4. HNC partial structure factor $S_{AA}(k)$ (left) and pair distribution function $g_{AA}(r)$ (right) for the LAM (set 1) at $V^* = 7.5$ (full curves) and for the BCM (set 4) at $\Gamma = 24$ (broken lines). The circles report x-ray diffraction data on liquid germanium at $T = 1253$ K from Waseda and Suzuki (1975).

presence of such a shoulder near freezing, becoming an asymmetry in the peak shape at appreciably higher temperatures (Gabathuler and Steeb 1979). We note from figure 3 that the position of the shoulder in $S_{AA}(k)$ lies in correspondence with the main peak in $S_{BB}(k)$. On further increase in V^* the shoulder grows into a strong peak at essentially unshifted position, while the former main peak is reduced to a prepeak at progressively lower wavenumbers. We shall return in § 4.2 below to discussing other aspects of the results in figure 3 in relation to the question of the quantitative accuracy of the HNC.

It would clearly be futile to aim at more than a qualitative comparison between theory and experiment. Nevertheless, we report in figure 4 the HNC results for $g_{AA}(r)$

and $S_{AA}(k)$ at $V^* = 7.5$ together with the liquid-structure data on germanium near freezing, from the x-ray diffraction experiments of Waseda and Suzuki (1975) (see also Waseda (1980)). We have tried to eliminate irrelevant noise from such a comparison by a suitable choice of σ_{AA}, leading to the model parameters in set 1 (table 1). Moderate changes of the values of the parameters around these preferred values do not alter the quality of the comparison appreciably. We note from the figure that the HNC solution of the model mimics the observed structure to a remarkable degree. Obviously, the discontinuity in $g_{AA}(r)$ at contact and the small peak in $g_{AA}(r)$ at $r = 2\sigma_{AA}$ are consequences of the hard-sphere schematisation and could easily be remedied by introducing appropriate soft-core repulsive potentials. The other points to be noted concern the shape of the main minimum and the second coordination shell in $g(r)$, as well as the dephasing of the oscillations in $S(k)$ at large k. While the latter could largely be remedied by adopting a slightly larger value for σ_{AA}, this would further smooth out the shallow minimum and the second coordination shell in $g_{AA}(r)$. The behaviour of $g_{AA}(r)$ that the model should show in this crucial region of interatomic distance is in fact rather poorly represented by the HNC, as we shall see immediately below.

4.2. Quantitative analysis of the liquid-structure theory

The quality of the HNC solution will now be discussed through comparisons with the corresponding HMSA solution and with the results of our Monte Carlo runs. All the calculations in this section refer to the amorphous state density and to the parameters of set 2 in table 1, where the tetrahedron rule has been somewhat relaxed. This choice for the density and for σ_{BB} is motivated by the need to accelerate the equilibration rate and to reduce the length of the sampling runs in the simulation, down to the still rather large numbers of steps stated in § 3.

Figure 5 shows the HNC results for $g_{\alpha\beta}(r)$ at $V^* = 5$ in comparison with the Monte Carlo results. It is seen that the HNC solution is still fully quantitative up to this value of the coupling strength, except in the values at hard-sphere contact (only partly shown in the figure). The HMSA solution is very similar to the HNC and to the data over this range of V^*.

Figure 6, on the other hand, shows that some quantitative discrepancies between theory and simulation arise already at $V^* = 7.5$. The present discussion, although based on figure 6, will also take account of tests that we have carried out at larger values of V^* and do not illustrate by means of figures. In general, we find that good quantitative agreement between HNC and simulation persists for $g_{AB}(r)$ and $g_{BB}(r)$ to large values of V^*. However, the HNC seriously underestimates the depth of the main minimum in $g_{AA}(r)$ and thus the stability of the first interatomic coordination shell that the model implies.

This defect of the HNC solution is not remedied by the HMSA, which in addition has the unpleasant feature of yielding a slightly negative value for $g_{AB}(r)$ at its main minimum. This is shown in figure 6 for $V^* = 7.5$, where thermodynamic consistency has been reached at the value $b = 1$ for the constant in the mixing function of (6). At appreciably larger values of V^*, the pressure in the HMSA drifts towards negative values, thus preventing a full implementation of the thermodynamic consistency requirement.

On the other hand, the HMSA has much better control on the low-k behaviour of the structure factors at very large values of V^*. This is shown in figure 3 at $V^* = 24$. It is seen there that the partial structure factors almost diverge at long wavelengths in the HNC, thus preventing the extension of this approximate theory to larger values of V^*. The

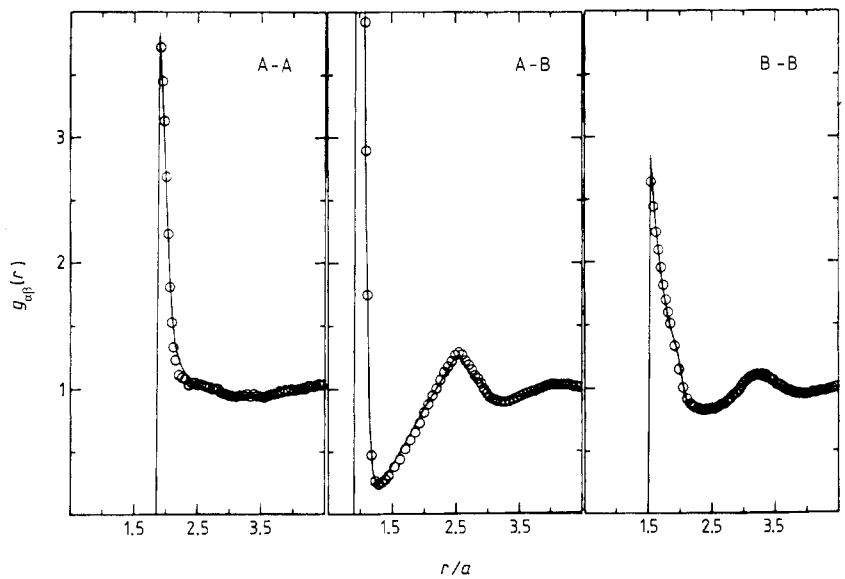

Figure 5. Partial pair distribution functions $g_{\alpha\beta}(r)$ in the LAM (set 2) at $V^* = 5$. Full lines, HNC results; circles, Monte Carlo results.

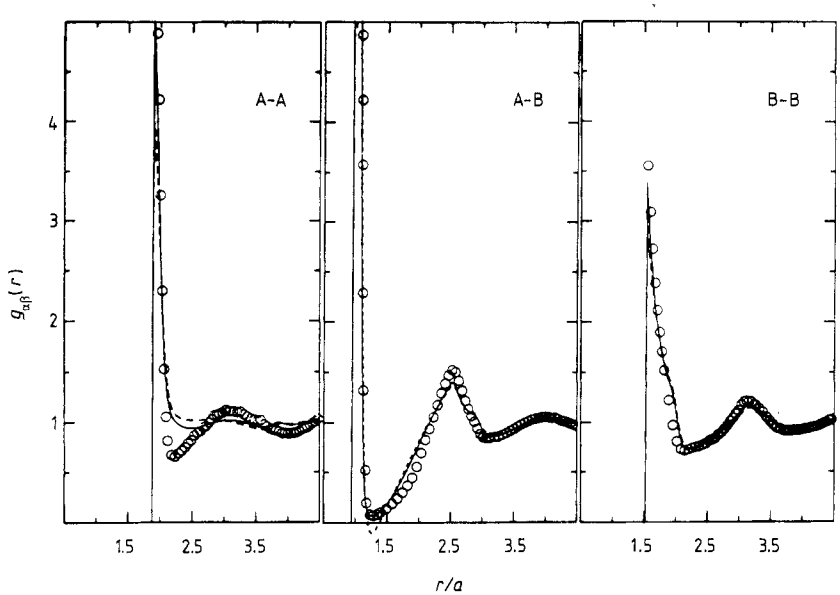

Figure 6. Partial pair distribution functions $g_{\alpha\beta}(r)$ in the LAM (set 2) at $V^* = 7.5$. Full lines, HNC results; broken lines, HMSA results corresponding to $b = 1$ as obtained from thermodynamic consistency; circles, Monte Carlo results.

HMSA structure factors have instead a reasonable behaviour at this and higher values of V^*, although full thermodynamic consistency cannot be achieved for the reason already given.

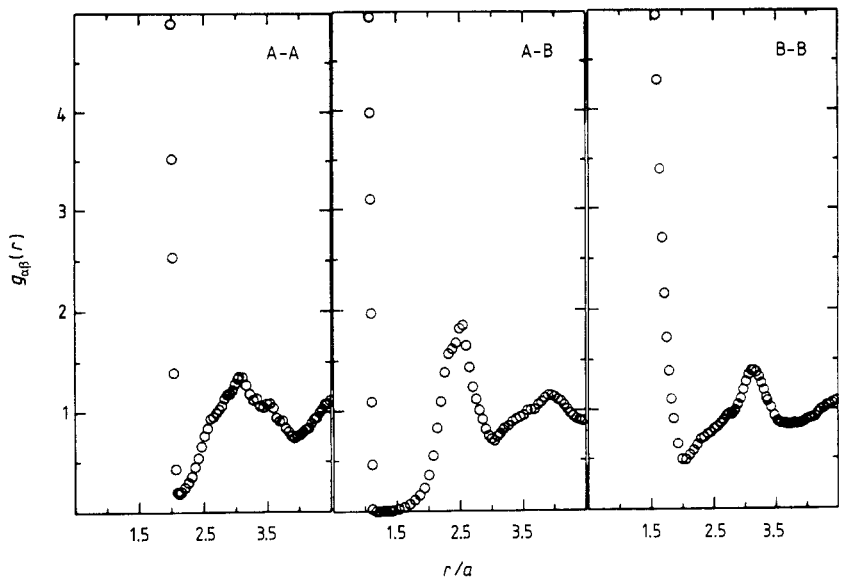

Figure 7. Monte Carlo results for the partial pair distribution functions $g_{\alpha\beta}(r)$ in the LAM (set 2) at $V^* = 22$.

4.3. Structure in supercooled liquid states in relation to amorphous germanium

The structural behaviour of the model at a large value of V^* is illustrated in figure 7 through Monte Carlo results obtained with set 2 of the parameters in table 1. Only qualitative comparison can be made with the diffraction data of Etherington *et al* (1982) on amorphous germanium, which refer to room temperature and a much lower density. Their data show complete stability of the first interatomic coordination shell ($g_{\mathrm{GeGe}}(r) \simeq 0$ at its main minimum) and a second interatomic coordination shell which is appreciably sharper than shown for $g_{\mathrm{AA}}(r)$ in figure 7. Presumably, closer contact with the data on the medium-range topology of the amorphous state could be made if the tetrahedron rule were more strictly enforced in the model. This would require much longer simulation runs or, preferably, an appropriate quantitative improvement of the HNC theory.

With regard to the A–A partial structure factor in strongly supercooled states, we may refer again at this point to the HNC and HMSA results shown in figure 3 for $V^* = 24$. We wish to draw specific attention to the position and shape of the prepeak in $S_{\mathrm{AA}}(k)$, in relation to the diffraction data on amorphous germanium. It is seen from figure 3 that the prepeak is somewhat sharper in the HMSA than in the HNC, but still considerably less resolved than in the experiment and located at $ka \simeq 3.1$ rather than at $ka \simeq 2.42$. Through purely empirical reshaping of the first two coordination shells in $g_{\mathrm{AA}}(r)$, guided by the Monte Carlo data in figure 7, we have found that the position of the prepeak in $S_{\mathrm{AA}}(k)$ can be shifted to values of ka which are even below the experimentally observed one. Thus the prepeak in the structure factor reflects the detailed nature of medium-range correlations, as Etherington *et al* (1982) have pointed out in the analysis of their data. It may be noted, on the other hand, that the longer-range interatomic correlations in space, as described by the positions of the successive peaks in $g_{\mathrm{AA}}(r)$, are in good approximate agreement with the diffraction data (Ferrante *et al* 1988).

Table 3. Coordination numbers and properties of the main minimum in the HNC pair distribution functions of the BCM (set 4).

Γ	N_{AB}	R_{AB}/d	$g_{AB}(R_{AB})$	N_{AA}	R_{AA}/d	$g_{AA}(R_{AA})$	N_{BB}	R_{BB}/d	$g_{BB}(R_{BB})$
0	6.32	1.07	0.85	10.2	1.60	0.85	11.1	1.30	0.82
5	4.73	0.94	0.79	10.6	1.62	0.88	11.3	1.31	0.80
10	3.89	0.86	0.65	10.4	1.61	0.90	10.9	1.29	0.78
15	3.61	0.82	0.50	9.26	1.55	0.93	9.98	1.25	0.74
20	3.47	0.79	0.39	7.64	1.46	0.96	9.33	1.22	0.71
24	3.43	0.77	0.31	6.62	1.40	0.96	8.93	1.20	0.68
43.5	3.46	0.73	0.09	5.05	1.30	0.87	7.77	1.13	0.55
58.7	3.53	0.71	0.03	4.70	1.27	0.79	7.46	1.10	0.48
65.4	3.55	0.71	0.03	4.71	1.27	0.77	7.45	1.10	0.46

5. Results for the BCM

As already mentioned in §1, we have carried out only HNC calculations for the bond charge model, following its structural evolution with increasing coupling strength Γ or equivalently increasing bond charge $|Z_B|$. The hard-sphere contact distances (set 4 in table 1) are the same as in set 3 for the LAM, except that σ_{AB} has been set equal to $d/2$ in order to preserve the location of the equilibrium position of the bond particles at the centre of the bond.

The main qualitative structural difference between the BCM and the LAM is that bond particle localisation and structural rearrangements with increasing A–B coupling strength proceed more smoothly in the former model. The localisation process is illustrated in table 3, which should be compared with table 2 for the LAM. We draw attention in particular to the behaviour of N_{AB} in table 3, showing a monotonic drop from $N_{AB} \simeq 6.3$ at $\Gamma = 0$ to $N_{AB} \simeq 3.5$ at large Γ. Similarly, the coordination number N_{AA} drops smoothly from $N_{AA} \simeq 10.3$ at $\Gamma = 0$ to $N_{AA} \simeq 6.6$ at $\Gamma = 24$, where contact with the properties of real liquid germanium appears to be made. At this and higher values of Γ, the behaviour of the BCM is qualitatively similar to that of the LAM. We conclude that the long-range part of the Coulomb interactions has essentially unimportant structural consequences once appreciable localisation of the bond particles is present.

The partial structure factors of the BCM at $\Gamma = 24$ are compared with those of the LAM at $V^* = 7.5$ in figure 4 (for A–A correlations) and in figure 8 (for A–B and B–B correlations). Again, only differences of quantitative detail are apparent between the two models at these values of their respective coupling strengths.

6. Melting criteria

We have seen in §§ 4 and 5 that the model liquid structure qualitatively resembles the structure of real liquid germanium when the coupling strength parameter takes the approximate values $V^* \simeq 7.5$ or $\Gamma \simeq 24$. Given the melting temperature and the density of germanium, these values are close to those anticipated in § 2 from the observed band gap E_g in the crystal ($E_g \simeq 0.7$ eV) and from the estimated value of the bond charge ($|Z_B| \simeq 2/\sqrt{\varepsilon_0}$, ε_0 being the dielectric constant of the crystalline material).

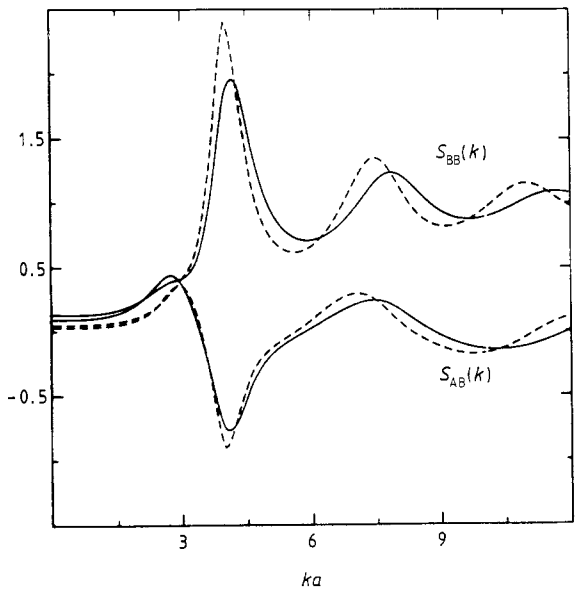

Figure 8. HNC partial structure factors $S_{AB}(k)$ and $S_{BB}(k)$ in the BCM (set 4) at $\Gamma = 24$ (full curves) and in the LAM (set 1) at $V^* = 7.5$ (broken curves).

We now ask whether there is any generality to these results. Namely, we ask whether, for semiconductors which melt with a break-up of chemical bonding, one can formulate melting criteria in the forms

$$E_g/k_B T_m \simeq \text{constant} \tag{7}$$

or

$$4e^2/(\varepsilon_0 a k_B T_m) \simeq \text{constant} \tag{8}$$

at the melting temperature T_m.

Figure 9 shows that both criteria are approximately satisfied for atmospheric pressure melting in group IV elements and group III–group V compounds. Figure 9 uses data on T_m, E_g, ε_0 and the density from *Landolt–Börnstein, New Series* (1982). The constants in (7) and (8) are found from the plots in figure 9 to be approximately equal to 10 and to 20, respectively. These values are in essential accord with the values of V^* and Γ obtained from our model for germanium near freezing.

7. Discussion and summary

We have examined in this work a statistical mechanical model for a special class of liquids, which is appropriate to work on the lattice dynamics of crystalline semiconductors and has qualitative relevance to the melting of these materials.

Relative to previous models in liquid-state theory the special new feature is the possibility of varying the degree of localisation of a component in the liquid and of building through it a degree of directionality in the effective interactions between the other components. It is clear from our results that established integral equation

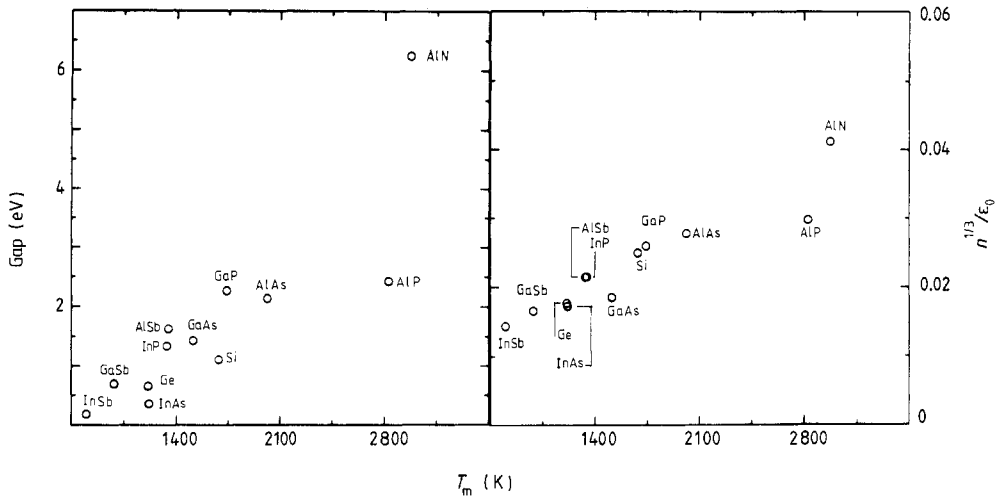

Figure 9. Correlation of the melting temperature T_m of elemental semiconductors and III–V compounds with the valence–conduction band gap E_g (left) and with the quantity $n^{1/3}/\varepsilon_0$ (right), where n is the number of atoms per unit volume and ε_0 the static dielectric constant of the crystal.

techniques of liquid-structure theory are still useful in this context, but cannot handle localisation and its consequences in a fully quantitative manner and may indeed break down when the model parameters are stretched very far. Further efforts at refining the theory for this type of model would seem to be worthwhile.

The specific results that we have presented provide a reasonable pseudoclassical scenario for the structural behaviour of ions and electrons in a molten semiconductor, as it is cooled from a very high temperature towards the freezing point. A qualitative prediction is that the degree of electron localisation in the melt near freezing is quite high. This feature is consistent with molten semiconductors being rather poor metallic conductors and is one of the points of interest in current developments in the study of molten silicon by the Car–Parrinello method (Stich 1988). Complete localisation occurs in our model in strongly supercooled states, but only imperfect contact can as yet be made with the observed medium-range topology of the atomic structure in amorphous germanium.

Finally, our approach has led us to suggest melting criteria for semiconductors, which we have seen to be empirically verified. The melting criterion involving the band gap is perhaps not unexpected, although we have not been able to find it already noted in the literature. The melting criterion based on the bond charge concept is less obvious for semiconductors and its empirical verification gives additional support to the qualitative usefulness of Phillips' idea.

Acknowledgments

This work was carried out under the auspices of the Ministero della Pubblica Istruzione and the Consiglio Nazionale delle Ricerche of Italy.

Note added in proof. After submission of this work, Professor J E Enderby drew our attention to work by Godefroy and Aigrain (1962), in which a melting criterion for semiconductors relating the melting temperature to the band gap was proposed and discussed.

References

Abernethy G M and Gillan M J 1980 *Mol. Phys.* **39** 839
Ashcroft N W and Langreth D 1967 *Phys. Rev.* **156** 685
Car R and Parrinello M 1988 *Phys. Rev. Lett.* **60** 204
Enderby J E and North D 1968 *Phys. Chem. Liquids* **1** 1
Etherington G, Wright A C, Wentzel J T, Dore J C, Clark J H and Sinclair R N 1982 *J. Non-Cryst. Solids* **48** 265
Ferrante A, Wang Li and Tosi M P 1988 *Phil. Mag.* A **58** 13
Gabathuler J P and Steeb S 1979 *Z. Naturf.* a **34** 1314
Gillan M, Larsen B, Tosi M P and March N H 1976 *J. Phys. C: Solid State Phys.* **9** 889
Glazov V M, Chizhevskaya S N and Glagoleva N N 1969 *Liquid Semiconductors* (New York: Plenum)
Godefroy L R and Aigrain P 1962 *Proc. Int. Conf. Physics of Semiconductors (Exeter)* p 234
Hafner J and Kahl G 1984 *J. Phys. F: Met. Phys.* **14** 2259
Kolafa J and Nezbeda I 1987 *Mol. Phys.* **61** 161
Landolt–Börnstein, New Series 1982 Group III, vol 17a (New York: Springer)
Luedtke W D and Landman U 1988 *Phys. Rev.* B **37** 4656
Martin R M 1969 *Phys. Rev.* **186** 871
Miglio L, Ruggeroni P, Benedek G and Colombo L 1988 *Phys. Scr.* **37** 768
Phillips J C 1970 *Covalent Bonding in Crystals and Molecules* (Chicago: University of Chicago)
Smith W R and Nezbeda I 1984 *J. Chem. Phys.* **81** 3694
Stich I 1988 private communication
Stillinger F H and Weber T A 1985 *Phys. Rev.* B **31** 5262
Ubbelohde A R 1978 *The Molten State of Matter* (Chichester: Wiley)
Viscor P 1988 *J. Non-Cryst. Solids* **101** 170
Waseda Y 1980 *The Structure of Non-Crystalline Materials* (New York: McGraw–Hill)
Waseda Y and Suzuki K 1975 *Z. Phys.* B **20** 339
Weber W 1977 *Phys. Rev.* B **15** 4789
Wertheim M S 1988 *J. Chem. Phys.* **88** 1145
Zerah G and Hansen J P 1986 *J. Chem. Phys.* **84** 2336